Supplemental Material

Orbital Angular Momentum Generation by a Point Defect in Photonic Crystals

Menglin L. N. Chen[1], Li Jun Jiang[1], and Wei E. I. Sha[2]

1. Electromagnetics and Optics Lab, Department of Electrical and Electronic Engineering, The University of Hong Kong, Hong Kong

2. College of Information Science and Electronic Engineering, Zhejiang University, Hangzhou, 310027, P. R. China.

Emails: jianglj@hku.hk (JIANG); weisha@zju.edu.cn (SHA)

1. Modal analysis by finite-difference method

We consider only the TM mode in a 2D PC. The governing equation for the 2D eigenvalue problem can be written as

$$\frac{1}{\bar{\epsilon}}\frac{\partial^2 E_z}{\partial x^2}+\frac{1}{\bar{\epsilon}}\frac{\partial^2 E_z}{\partial y^2}+k_0^2 E_z=0 \tag{1}$$

where k_0 is the free-space wavenumber and $\bar{\epsilon}$ is the averaged dielectric constant.

For the band-structure calculation, each unit cell is divided into many grids as shown below. Here, the lattice constant P_x is equal to P_y for square unit cell. $\phi_{m,n}$ $(m,n=1,2,3,...N)$ denotes the electric field E_z at each sampling point. Due to the periodicity, each unit cell has $N\times N$ unknowns. The Floquet or Bloch boundary conditions should be imposed at the boundaries, i.e.

$$\phi_{m,N+1}=\phi_{m,1}e^{jk_xP_x},\quad \phi_{N+1,n}=\phi_{1,n}e^{jk_yP_y} \tag{2}$$

where k_x and k_y are the Bloch wavenumbers in the lattice.

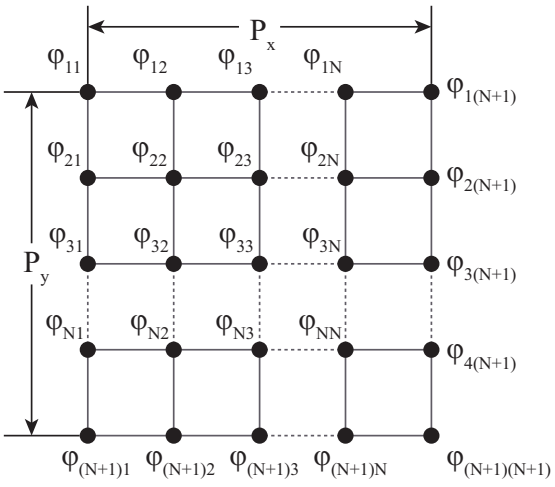

Fig. S1. One unit cell with finite-difference grids.

To simulate curved boundaries of the cylindrical rods, considering the tangential E_z component is continuous across the air-dielectric interface, the averaged dielectric constant is of the following form,

$$\bar{\epsilon}=\epsilon_{m,n}=\frac{1}{4}(\epsilon_{m-0.5,n-0.5}+\epsilon_{m+0.5,n-0.5}+\epsilon_{m-0.5,n+0.5}+\epsilon_{m+0.5,n+0.5}) \tag{3}$$

Finite-difference approximation of the differential eigenvalue equation is given by,

$$\frac{1}{\epsilon_{m,n}}\frac{\phi_{m,n+1}+\phi_{m,n-1}-2\phi_{m,n}}{\Delta x^2}+\frac{1}{\epsilon_{m,n}}\frac{\phi_{m+1,n}+\phi_{m-1,n}-2\phi_{m,n}}{\Delta y^2}=\left(\frac{\omega}{c}\right)^2\phi_{m,n} \tag{4}$$

Then, we can recast the differential eigenvalue equation into a matrix form,

$$M\Phi=\left(\frac{\omega}{c}\right)^2\Phi,\quad \Phi=(\phi_{11}\ \phi_{12}\ \ldots\ \phi_{1N}\ \phi_{21}\ \phi_{22}\ \ldots\ \phi_{2N}\ \ldots\ \phi_{N1}\ \phi_{N2}\ \ldots\ \phi_{NN})^T \tag{5}$$

where M is a sparse matrix with $N^2\times N^2$ dimensions. The above can be solved by a standard eigenvalue solver in MATLAB.

By sweeping k_x and k_y along the edge of the irreducible Brillouin zone, we can solve the corresponding eigenvalue (mode frequency) and eigenvector (eigenmode). By connecting the eigenvalues to each k_x and k_y pair, we can build the band structure of the periodic lattice. The numerical results of the PC with the same geometry and parameters in the manuscript are plotted below.

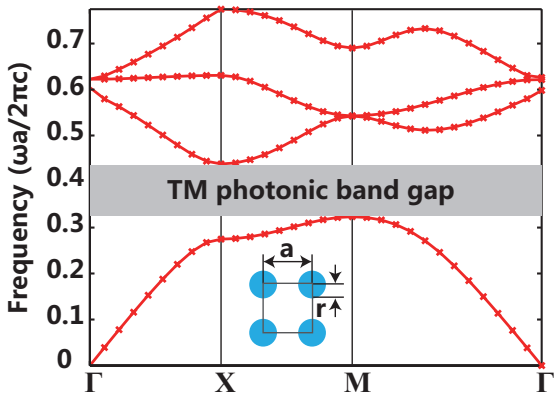

Fig. S2. A 2D PC and its band structure. The PC consists of dielectric rods in a square lattice with the lattice constant $a=12$ mm. The rods with the dielectric constant of $\epsilon_r=8.5$ and radius of $r=0.2a$ mm are placed in the air background. We show the first four bands of the TM mode. A photonic band gap opens up between the first and second bands and forbidden frequencies range from $0.3236c/a$ to $0.4328c/a$, where c is the speed of light in vacuum.

For the modal analysis of the localized mode around a point defect in a 2D PC, we use a supercell consisting of 5×5 unit cells. The central rod in the supercell is the defect rod and the others are ideal bulk rods. The band structure when the radius of the defect rod $r_d=0.6a$ is shown below. Within the bandgap, we find the eigenvalues and eigenvectors, which correspond to the defect modes. Due to translation symmetry breaking along both the x and y directions, eigenvalues and eigenvectors are the same at different points along the edge of the irreducible Brillouin zone.

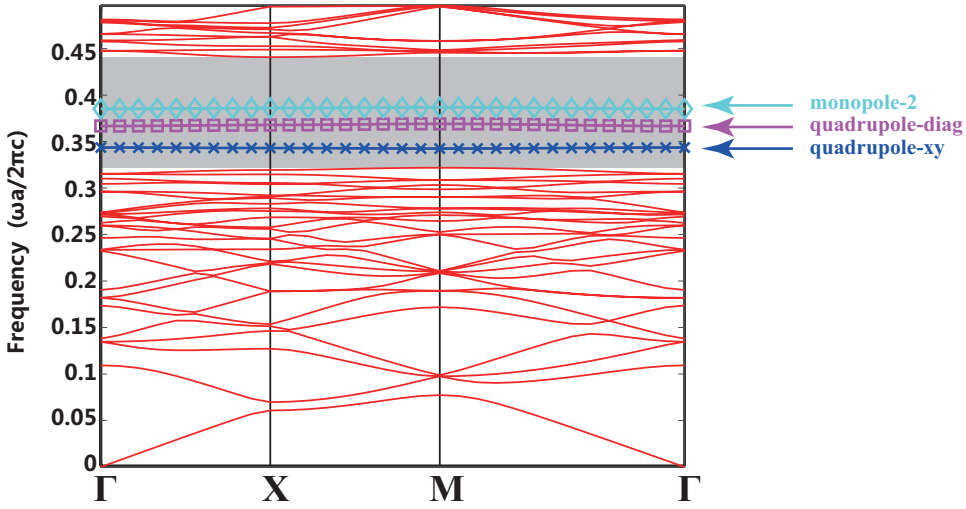

Fig. S3. The band structure of the 2D PC with a point defect. Three defect modes have been found when $r_d = 0.6a$. Arranged from lowest to highest eigenfrequencies, they are the quadrupole-xy, quadrupole-diag and monopole-2 modes.

2. Simulation results for quadrupole defect states

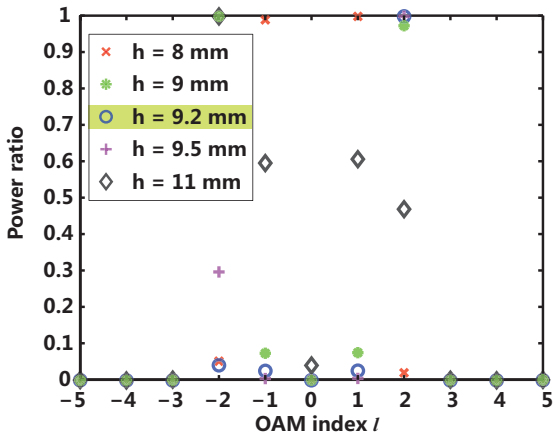

Fig. S4. The evolution of the radiated E_z above the 3D PC with varying height of the PC. The highlighted result is for the case with the optimized parameters, same as the parameters in Fig. 5. As for the influence of finite height, we can see the decrease in height tends to push the mode down to the dipole shape and correspondingly, increase in height will pull the mode up to the monopole-2 state.

Parameters	8.8 GHz	230 THz
Lattice constant, a	12 mm	458.4 nm
Radius of bulk rods, r	2.5 mm	95.5 nm
Radius of defect rod, r_d	7.2 mm	275.0 nm
Radius of scatterer, r_s	1.65 mm	63.5 nm
Radius of the circular opening, r_c	9.5 mm	363.0 nm
Height of rods, h	9.2 mm	350.0 nm

Table S1. Original and scaled parameters of the structure with a quadrupole defect. The original metallic plates are considered as the PEC (perfect-electric-conductor) boundary with no thickness. Therefore, the scaling law is not applicable to the two metallic plates. In the scaled structure, aluminum plates are used and their thickness have been optimized to obtain desired results and the resultant $h = 50$ nm. Dispersion of aluminum has been taken into consideration.

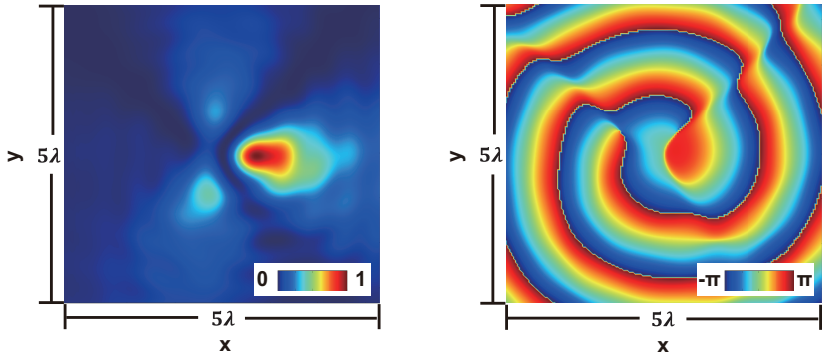

Fig. S5. Simulated intensity and phase distributions of the E_z component at a transverse plane of 1000 nm above the scaled structure. Due to the dispersion of the aluminum, the operating frequency is shifted to 224.5 THz.

3. Simulation results for dipole defect states

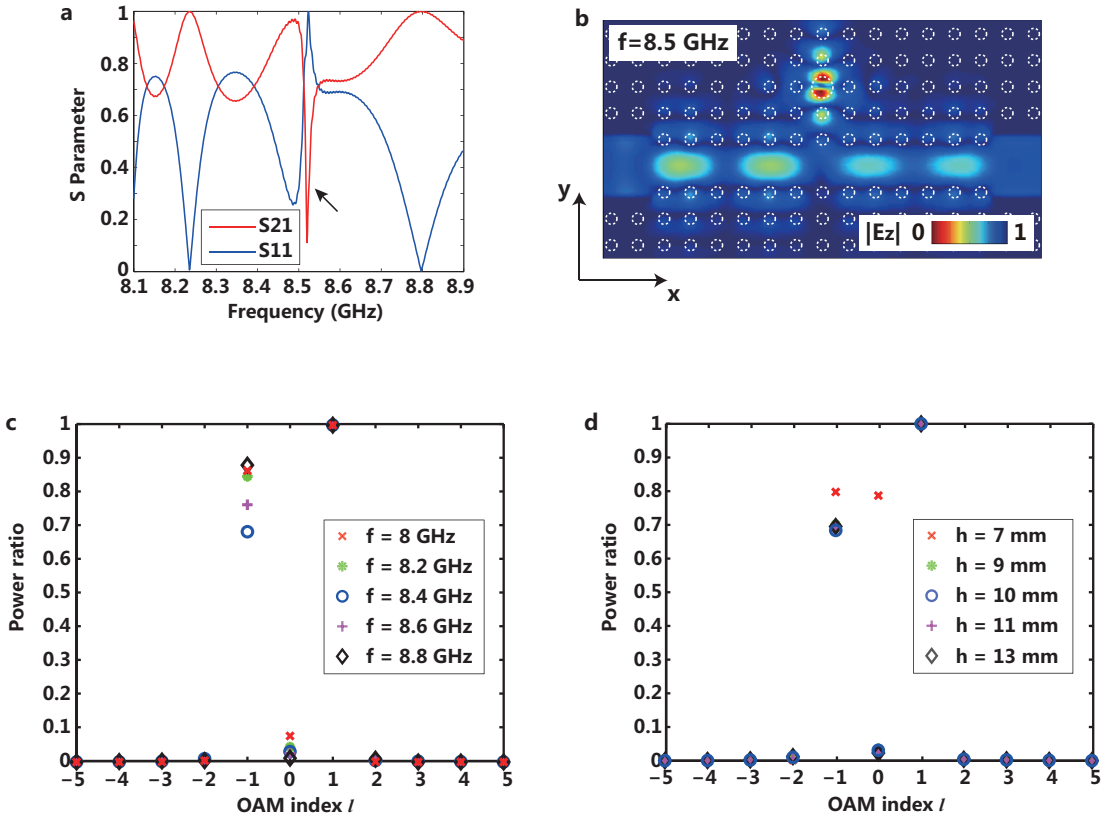

Fig. S6. Excited dipole states inside a 2D PC and evolution of the radiated E_z above the 3D PC with the defect rod of rotational symmetry. (a) The simulated scattering parameter for a 2D PC. Since the dipole states are degenerate states, we can only see one resonance around 8.5 GHz. According to the numerical results in Fig. 2, the mode frequency for the two modes is $0.3389c/a$, i.e. 8.47 GHz, which is consistent with the simulation results here. (b) The dipole state inside a 2D PC. (c,d) The projection of the complex field above the 3D PC onto the orthonormal basis of $e^{il\phi}$ along the azimuthal direction. The results are plotted with varying (c) frequency and (d) height of the PC. We can see due to the degeneracy of the dipole states, the capability of tuning the two states is very limited. The desired weights and phase factor of the two dipole states for generating a rotational mode cannot be obtained, by adjusting the frequency or the height of the 3D PC.

4. Generation of OAM of order ±1 and ±2

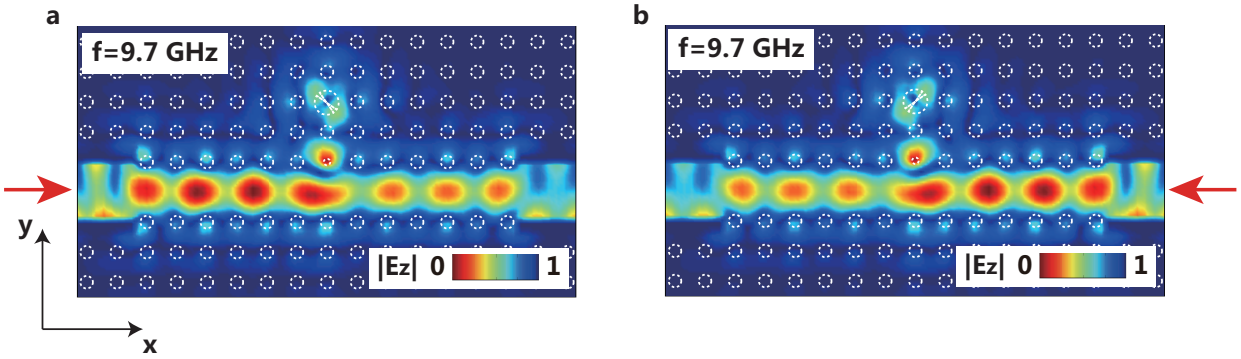

Fig. S7. Excited dipole states for generating OAM of order ±1 with different feeding ports and defect orientations.

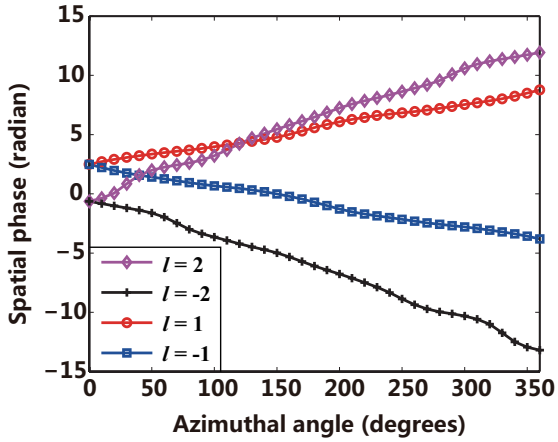

Fig. S8. The simulated phase distributions of radiated E_z along the azimuthal direction at a transverse plane of 30 mm above the 3D PC.

5. Experiment details

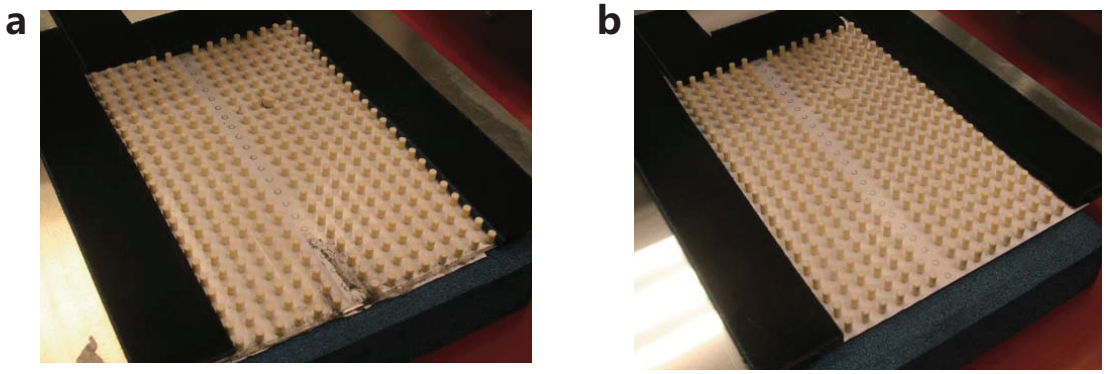

Fig. S9. Assembled PC samples. (a) The assembled PC sample with the dipole defect. (b) The assembled PC sample with the quadrupole defect.